Evidence for ordered magnetic moments at oxygen sites in antiferromagnetic Sr₂IrO₄ and Sr₃Ir₂O₇

M. Miyazaki,[1] R. Kadono,[1,2,*] M. Hiraishi,[1] A. Koda,[1,2] K. M. Kojima,[1,2] K. Ohashi,[3] T. Takayama,[4] and H. Takagi[4,5]

[1]*Muon Science Laboratory and Condensed Matter Research Center, Institute of Materials Structure Science, High Energy Accelerator Research Organization (KEK), Tsukuba, Ibaraki 305-0801, Japan*

[2]*Department of Materials Structure Science, Graduate University for Advanced Studies, Tsukuba, Ibaraki 305-0801, Japan*

[3]*Department of Advanced Materials, Graduate School of Frontier Sciences, University of Tokyo, Kashiwa, Chiba 277-8561, Japan*

[4]*Max Planck Institute for Solid State Research, Heisenbergstrasse 1, 70569 Stuttgart, Germany*

[5]*Department of Physics, Graduate School of Science, University of Tokyo, Tokyo 113-0033, Japan*

In this study, the magnetic ground state of iridium perovskites ($Sr_{n+1}Ir_nO_{3n+1}$, where $n = 1, 2$, and ∞) was considered using muon spin spectroscopy (μSR). When probed by muons in Sr_2IrO_4 and $Sr_3Ir_2O_7$ ($n = 1,2$), the internal field (B_{loc}) showed clear signs of a magnetic order in two stages at transition temperatures $T_N \simeq 230$ K and $T_m \simeq 90$ K in Sr_2IrO_4 and $T_N \simeq 280$ K and $T_m \simeq 70$ K in $Sr_3Ir_2O_7$. In contrast, no long-range magnetic order was observed in orthorhombic $SrIrO_3$ ($n = \infty$). Based on the known magnetic structure in Sr_2IrO_4 and $Sr_3Ir_2O_7$, we successfully identified muon sites in these compounds from the magnitude of B_{loc} in the first stage ($T_m \leqslant T \leqslant T_N$). Below T_m, B_{loc} probed by a fraction of muons occupying sites near the apical oxygen of IrO_6 octahedra exhibited a further increase but remained mostly unchanged for sites close to the in-plane oxygen. While such behavior cannot be explained by the alteration of the Ir spin structure, it is consistent with the selective appearance of ordered magnetic moments on the apical oxygen. The oxygen polarization was also in line with the reported magnetization anomalies in these compounds below $\sim T_m$. A possible link between the oxygen polarization and ferroelectric (multiferroic) behavior in Sr_2IrO_4 was considered.

I. INTRODUCTION

Layered iridium perovskites (Ruddlesden-Popper series: $Sr_{n+1}Ir_nO_{3n+1}$, where $n = 1, 2, ...$) serve as an intriguing playground for exploiting the novel properties of d electrons arising from competition between the spin-orbit (SO) interaction, crystal field, and Coulomb interaction (electronic correlation) of comparable energy in $5d$ transition metal oxides. Recent studies with a variety of microscopic probes have established that the monolayer compound Sr_2IrO_4 is a Mott insulator realized within t_{2g} manifolds that are reorganized by the SO interaction: the t_{2g} band splits into two narrow subbands mainly composed of $J_{eff} = 3/2$ and $J_{eff} = 1/2$ spin-orbital states, where the latter is further split by the Coulomb interaction (U) into upper and lower Hubbard bands upon half filling [1,2]. The bandwidth (W) increases with the number of IrO layers (n), which leads to the suppression of the Mott transition ($W > U$) and emergence of an anomalous metallic state in $SrIrO_3$ [3].

Regarding magnetic properties, Sr_2IrO_4 is known to exhibit weak ferromagnetism below the Curie temperature $T_C \simeq 230$ K in accordance with the Mott-insulating phase, which is characterized by small saturation moments ($\mu_s \sim 0.1\mu_B/$Ir) [4–6]. This is now understood to come from a canted antiferromagnetic (AF) order within the IrO_2 (ab) plane [1,7,8], where the spin canting is induced by the strong SO interaction mapped onto the pseudodipolar interaction and the Dzyaloshinsky-Moriya interaction between the $J_{eff} = 1/2$ isospins [9]. While similar behavior has been reported for $Sr_3Ir_2O_7$ ($\mu_s < 0.04\mu_B/$Ir) [10], recent studies using resonant x-ray scattering have shown that the magnetic structure is a

G-type AF [11] with c-axis collinear moments [12,13], where the spin flop from Sr_2IrO_4 to $Sr_3Ir_2O_7$ is attributed to the three-dimensional (cubic) character of the $J_{eff} = 1/2$ ground state that mediates the interlayer pseudodipolar interaction common to the in-plane [12].

However, these compounds exhibit complicated magnetic properties at low temperatures (and under weak magnetic fields) that do not necessarily fit into the current framework of effective theory. Recent studies on Sr_2IrO_4 have revealed a magnetic anomaly at low temperatures that is quite sensitive to an external field. The magnetization is anomalously reduced below $T_M \sim 110$ K at 0.05 T (where T_M is reduced to ~ 50 K at 0.15 T), which suggests an enhanced antiferromagnetic correlation below T_M [14,15]. The anomaly has also been shown to be closely linked with the charge sector; the dielectric response exhibits crossover from relaxor-like to ferroelectric behavior as the temperature is decreased past T_M. These features correlate with the reduction in the Ir-O-Ir bond angle, which suggests a change in spin canting induced by alteration of the exchange coupling. While the situation is not as clear for $Sr_3Ir_2O_7$, earlier reports in the literature have reported the observation of a rapid decease in magnetization at $T_D \simeq 50$ K and reversal in the basal plane below 20 K under field-cooled conditions at 0.01 T. This has only been observed at low magnetic induction (below ~ 0.2 T) [10,15]. Again, these anomalies exhibit a certain correlation with the charge sector as inferred from the sharp increase in the electrical resistivity [10,14,15].

In contrast to these two cases, no clear anomaly suggesting a phase transition has been observed in the bulk properties of orthorhombic $SrIrO_3$ ($n = \infty$) over the temperature range from ambient to the liquid helium temperature. The electrical resistivity is metallic above ~ 45 K, where it exhibits a minimum, and changes to localizing behavior at lower

_____

*Corresponding author: ryosuke.kadono@kek.jp

temperatures [16]. In addition, a positive magnetoresistance has been observed below ~170 K [16]. Through a band calculation considering the SO interaction and optical conductivity, the carrier has been inferred to have a large effective mass due to electronic correlation [3].

Muon spin spectroscopy (μSR) is a unique probing technique for investigating the *local* magnetic structure and spin dynamics with extreme sensitivity, which is useful for studying magnetism arising from Ir moments to which neutron diffraction techniques are difficult to apply because of the large neutron absorption cross section of Ir nuclei. In particular, once the muon site(s) in the relevant compound is confirmed, the local magnetic field probed by the muon serves as a true measure of the order parameter because it is directly proportional to the magnitude of local magnetic moments. Note that the information gained from μSR is complementary to that from diffraction-based techniques (x-ray and neutron scattering), as the latter correspond to the information averaged over an entire crystal volume.

In this paper, we report μSR measurements on powder samples of $Sr_{n+1}Ir_nO_{3n+1}$ ($n = 1, 2,$ and ∞) under a zero external field that establish the development of a long-range magnetic order in Sr_2IrO_4 (T_N defined by "onset" $\approx$230 K) and in $Sr_3Ir_2O_7$ ($T_N \simeq$ 280 K). More importantly, we demonstrate the presence of a secondary magnetic phase at lower temperatures (below $T_m \simeq$ 90 K in Sr_2IrO_4 and $T_m \simeq$ 70 K in $Sr_3Ir_2O_7$) that can be discerned by the increase in spontaneous local fields at muon sites located near the apical oxygen of the IrO_6 octahedron. This result provides a microscopic basis for understanding the magnetic anomalies observed in the bulk properties of these compounds below T_m and suggests that the order parameter of the secondary magnetic phase is not solely determined by the magnitude of Ir local moments. We show that the μSR result below T_m is consistently reproduced by postulating the presence of small ordered moments at the apical oxygen in those two compounds, which is in line with the above anomalies in their bulk properties. Meanwhile, the absence of magnetism for $n = \infty$ supports the scenario that the t_{2g} bandwidth is a monotonic function of the coordination number in this series of Ir perovskites.

II. EXPERIMENT

A. Specimen

Polycrystalline samples (mosaic of small single crystals) of Sr_2IrO_4 and $Sr_3Ir_2O_7$ were prepared using a flux method (with $SrCl_2$ as the flux), while the orthorhombic phase of $SrIrO_3$ was obtained by synthesis under a high pressure of 5 GPa [17,18]. Structural analysis was performed using the powder x-ray diffraction technique to confirm that these samples mostly comprised a single phase with negligible content of impurities. The present samples of Sr_2IrO_4 and $Sr_3Ir_2O_7$ were prepared in the same batch as those measured by Fujiyama *et al.* using resonant x-ray diffraction [13]. The bulk properties of these samples were investigated with different methods, including measurements of the magnetization, electrical resistivity, Hall coefficient, and specific heat, to ensure the sample quality. Figure 1 shows the results of the magnetization measurements.
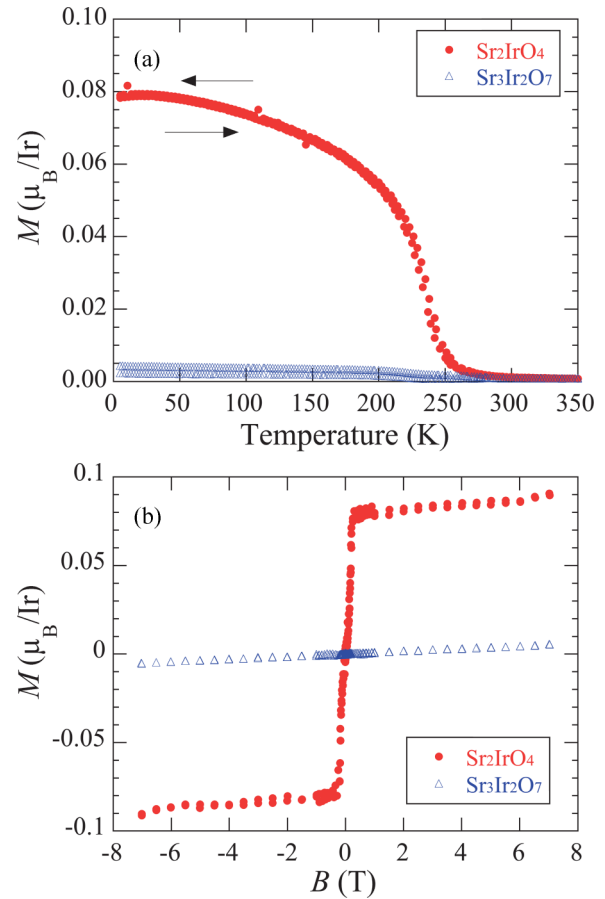

FIG. 1. (Color online) Magnetization (M) of Sr_2IrO_4 and $Sr_3Ir_2O_7$ samples used for μSR measurements (quoted from Ref. [13]). (a) M vs temperature, where measurements were made after zero-field cooling to 5 K with a sequence of (1) warming up to 350 K under a field $H = 1$ T parallel to the *a* axis and (2) then cooling down to 5 K. (b) M vs external field measured at 5 K ($H \parallel a$).

Figure 1(a) clearly shows that a weak ferromagnetic behavior developed below ~250 K in Sr_2IrO_4, which is consistent with earlier reports [4–6]. This is now understood to come from the canted Ir moments that exhibit a metamagnetic transition at ~0.2 T [2]. Meanwhile, $Sr_3Ir_2O_7$ exhibited much lower magnetization, although the temperature dependence was similar to that in Sr_2IrO_4. $Sr_3Ir_2O_7$ crystals are known to occasionally contain IrO_2 monolayers (corresponding to Sr_2IrO_4) as an impurity phase. Thus, the low magnetization in $Sr_3Ir_2O_7$ may be attributed to such an impurity phase; its fractional yield was empirically estimated to be less than 0.1% in single crystals [19].

In contrast, the magnetic susceptibility in the orthorhombic $SrIrO_3$ was found to be mostly independent of temperature ($\chi \simeq 3.3 \times 10^{-4}$ emu/mol at 1 T, except for divergent behavior at low temperatures that may be attributed to paramagnetism associated with weak localization below ~45 K). The behavior is understood to be Pauli paramagnetism [17]. Because the electronic specific coefficient is close to that of conventional metals ($\gamma = 2$–5 mJ/mol K^2), the compound has a Wilson ratio $R_w = 9.8$ that is much greater than the limit of strong correlation ($R_w = 2$) [17]. Such behavior is consistent

with earlier reports [16] and was attributed to a large Van Vleck term or strong magnetic correlation.

B. μSR experiment and data analysis

Conventional μSR measurements were performed using the LAMPF spectrometer installed on the M15/M20 beamlines at TRIUMF, Canada. During measurements under a zero external field (ZF), the residual magnetic field at the sample position was reduced to below 10^{-6} T, while the initial muon spin direction was parallel to the muon beam direction $[\vec{P}_\mu(0) \parallel \hat{z}]$. For longitudinal field (LF) measurements, a magnetic field was applied parallel to $\vec{P}_\mu(0)$. Time-dependent muon polarization $[G_z(t) = \hat{z} \cdot \vec{P}_\mu(t)]$ was monitored by measuring the decay-positron asymmetry along the $\hat{z}$ axis:

$$A(t) \simeq A_0 G_z(t) = \frac{N_+(t) - \alpha N_-(t)}{N_+(t) + \alpha N_-(t)}, \tag{1}$$

where A_0 is the average asymmetry.

$$N_\pm(t) = N_\pm(0) e^{-t/\tau_\mu}[1 \pm A_\pm G_z(t)]$$

is the positron event rate for the detector placed in the forward $(+)$ or backward $(-)$ position relative to the sample, τ_μ is the muon decay lifetime $(= 2.198 \times 10^{-6}$ s), $A_\pm$ is the decay positron asymmetry for the detector in question $(A_\pm \simeq A_0)$, and α is the instrumental asymmetry $[\alpha = N_+(0)/N_-(0) \simeq 1$ under normal conditions].

Figure 2 shows several examples of time-dependent ZF/LF-μSR asymmetry spectra and their fast Fourier transform (FFT) in $Sr_{n+1}Ir_nO_{3n+1}$; those for $n = 1$ and 2 exhibit a clear sinusoidal oscillation below T_C. Such a signal indicates the onset of a relatively homogeneous internal field at muon sites in accordance with the long-range magnetic order. The absence of enhanced muon depolarization just above T_C (usually expected as a consequence of the critical slowing down of the spin fluctuation) and the volumetric expansion of fraction for the magnetically ordered region below T_C (as inferred from the increase in oscillation amplitude with decreasing temperature) suggest that the transition is driven not by the magnetic interaction but by the Mott transition. In contrast, the spectra in $SrIrO_3$ ($n = \infty$) did not exhibit spontaneous oscillation over the entire observed range of the temperature, which demonstrates that no long-range magnetic order is present above 2 K.

More interestingly, closer investigation of the spectra for the former two cases revealed a secondary frequency component at lower temperatures, which can be clearly observed in the Fourier transform shown in Figs. 2(d) and 2(e). The signal amplitude of the secondary component increased instead of the first one, which suggests the gradual development of the former with decreasing temperature. Considering this, we analyzed the ZF-μSR time spectra by curve fitting using the following model function which is valid for the ordered phase of polycrystalline samples:

$$A(t) \simeq \sum_{i=1}^m A_i \left[\frac{1}{3} e^{-\lambda_L t} + \frac{2}{3} G_z(t, \Delta) e^{-\lambda_i t} \cos(\omega_i t + \phi) \right]$$
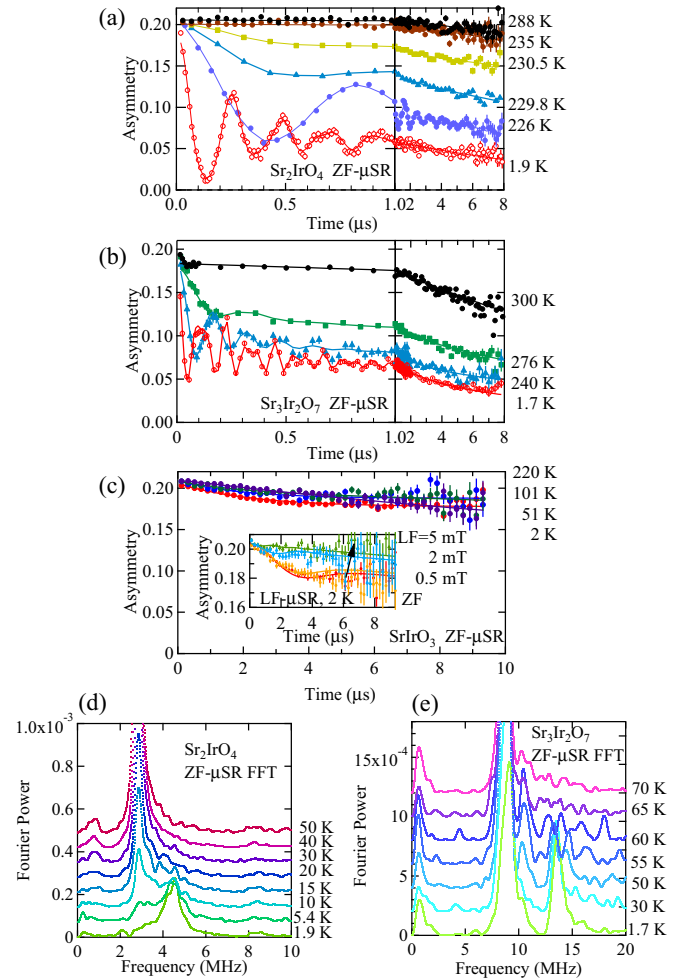$$+ A_{para} G_z(t, \Delta), \tag{2}$$

FIG. 2. (Color online) Typical μSR time spectra under zero external field (ZF) in (a) Sr_2IrO_4, (b) $Sr_3Ir_2O_7$, and (c) $SrIrO_3$, with inset showing some spectra under longitudinal field (LF). Modulation of sinusoidal pattern due to overlap of signals with different frequencies [$\sim$4.5 MHz and $\sim$8 MHz at 1.9 K in (a), $\sim$9 MHz and $\sim$13 MHz at 1.7 K in (b)] can be clearly observed in the earlier time range of the spectra up to 1 μs. Fast Fourier transform of ZF-μSR time spectra is shown for (d) Sr_2IrO_4 and (e) $Sr_3Ir_2O_7$. (f) LF-μSR spectra in $Sr_3Ir_2O_7$.

where $G_z(t, \Delta)$ is the Kubo-Toyabe relaxation function [20] to describe the slow Gaussian depolarization due to random local fields exerted from *nuclear* magnetic moments (with $\Delta \leqslant 10^{-1}$ μs^{-1} being the linewidth in the quasistatic limit), A_i is the partial asymmetry for the magnetic phase (with $\sum_i A_i = A_{mag}$), A_{para} is the asymmetry for the paramagnetic phase, λ_L is the longitudinal relaxation rate, λ_i is the transverse relaxation rate, ω_i is the muon spin precession frequency $(= 2\pi f_i = \gamma_\mu B_i$ with $\gamma_\mu = 2\pi \times 135.53$ MHz/T and B_i being the local field at the muon site), and ϕ is the initial phase of precession. Note that the first term in Eq. (2) represents the situation where the Kubo-Toyabe depolarization would be quenched [i.e., $G_z(t, \Delta) \simeq 1$] for one-third of the implanted muons exposed to a longitudinal internal field in the magnetic phase. We found that four components ($m = 4$) were sufficient to describe the spectra observed in Sr_2IrO_4. Similarly, the spectra in $Sr_3Ir_2O_7$ required four components
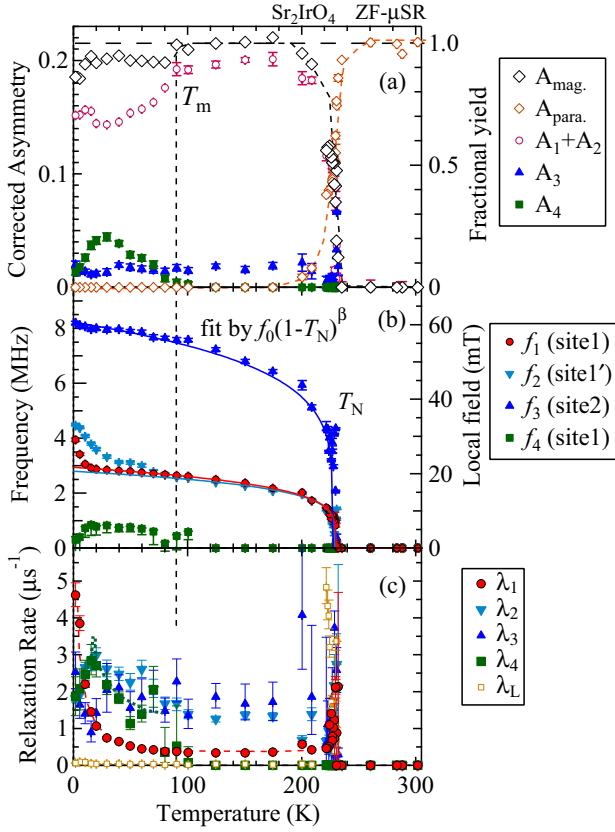
FIG. 3. (Color online) Temperature dependence of (a) partial asymmetry A_i, A_{para}, (b) muon precession frequency f_i, and (c) relaxation rate λ_i, λ_L in Sr$_2$IrO$_4$. Solid curves are results of curve fitting by $f_0(1 - T/T_N)^\beta$, and dashed curves are visual guides. For the correspondence between f_i and muon sites, see Fig. 6.

with one showing no oscillation, while one of the rest showed further splitting ($m = 5$) when $T \leqslant T_m$.

III. RESULT

A. Sr$_2$IrO$_4$

Figure 3 shows the partial asymmetry (A_i, A_{para}), muon precession frequency (f_i), and relaxation rate (λ_i) as determined from the curve fitting of ZF-μSR spectra in Sr$_2$IrO$_4$ as a function of temperature. As discussed below, the splitting

of signals into multiple frequencies can be attributed to the statistical distribution of implanted muons into magnetically inequivalent interstitial sites in the unit cell (situated at the local minima of electrostatic potential), where muons are exposed to different internal fields. The muon-electron hyperfine interaction is predominantly determined by the short-range magnetic dipolar interaction; thus, it strongly depends on the local configuration of the nearest-neighboring magnetic ions. The onset temperature (T_N) for the two precessing components f_1 ($= f_2$ for $T > T_m$) and f_3 agreed well with the $T_C \simeq 240$ K suggested by bulk magnetization [4–6]. T_N also perfectly matched with the values inferred from resonant x-ray diffraction (RXD) [2]. Curve fitting of the frequency by the power law $f_i(T) = f_{(0)i}(1 - T/T_N)^\beta$ yielded the critical index $\beta \simeq 0.2$ (see Table I for more details) which is situated somewhere between the three-dimensional (3D) Heisenberg ($\beta = 0.365$) and two-dimensional (2D) Ising ($\beta = 0.125$) spin systems. Note that β is distinctly smaller than that observed by RXD [2] and neutron [8] [$\beta \simeq 0.35$ ($\equiv 2\beta$ in Ref. [8])], which may be attributed to the volumetric expansion of magnetic domains with decreasing temperature as suggested by μSR (see A_i in Fig. 3). The intensity of x-ray/neutron diffraction should be proportional to the product of f_i ($\propto$ the true order parameter) and A_i ($\propto$ volumetric fraction of magnetic domains). Thus, precautions must be taken when interpreting diffraction data in terms of critical indices for the magnetic order parameter.

Nonetheless, the most salient feature in Fig. 3 is the gradual departure of $f_{1,2}$ from the curve predicted by the power law and further splitting into two frequencies ($f_1 < f_2$) below $T_m \simeq 90$ K; it shows a much steeper increase as the temperature decreases below 20–30 K. A corresponding behavior is suggested for f_3, for which the relaxation rate increased below T_m. An additional component ($i = 4$) showing strongly damped precession ($\lambda_4 \geqslant f_4$) also developed. The signal was accompanied by a loss of the initial asymmetry (seen from the reduction of A_{mag} by $\sim$10%, suggesting fast depolarization over a time range of 10^{-9} s). A similar μSR result was reported in a previous paper with some different details with regard to the behavior of fitting parameters [21].

Surprisingly similar behavior has previously been observed for the muon precession frequency in another Ir perovskite Ba$_2$IrO$_4$, except for the minor difference that the signal corresponding to f_3 is missing [22]. The difference may be due to the difficulty in identifying the precession signal of relatively

TABLE I. Muon spin precession frequency (extrapolated to $T = 0$ by curve fitting using the form $f_{(0)i}(1 - T/T_N)^\beta$ for $T_m \leqslant T \leqslant T_N$, where T_N is the Néel temperature) and corresponding internal field (B_i) in the AF phase of Sr$_2$IrO$_4$. T_N and the critical index β are determined by the fitted curves. The Ir moment size is estimated using the equation $\mu_{Ir} = B_i/\overline{B}_{loc}$, where $\overline{B}_{loc}$ is the field calculated for the Ir moment size of $1\mu_B$. Muon sites were assigned by searching for the positions of local potential minima around oxygen (with a distance of 0.1 nm), where the corresponding μ_{Ir} falls within a variation of 10% from the known value of $0.4\mu_B$. (The position is given in polar coordinates with the $\hat{z}$ axis parallel to the crystalline c axis.) O1: apical oxygen (0.5, 0.25, 0.2047); O2: in-plane oxygen (0.2001, 0.4501, 0.125); O2': in-plane oxygen (0.7001, 0.5499, 0.125).

Site	i	$f_{(0)i}$ (MHz)	B_i (mT)	T_N (K)	β	μ^+ position (θ, ϕ)	$\overline{B}_{loc}$ (mT/μ_B)	μ_{Ir}
1	1	2.941(3)	21.70(2)	230.1(1)	0.211(1)	O1+(60°, 45°)	51.6	0.4205(4)μ_B
1'	2	2.79(4)	20.6(3)	229.0(2)	0.192(5)	O1+(60°, 135°)	53.0	0.389(6)μ_B
2	3	8.22(4)	60.6(3)	227.4(3)	0.190(7)	O2+($\sim$16°, 45°)	142.4	0.426(2)μ_B
2'						O2'+($\sim$16°, 135°)	162.1	

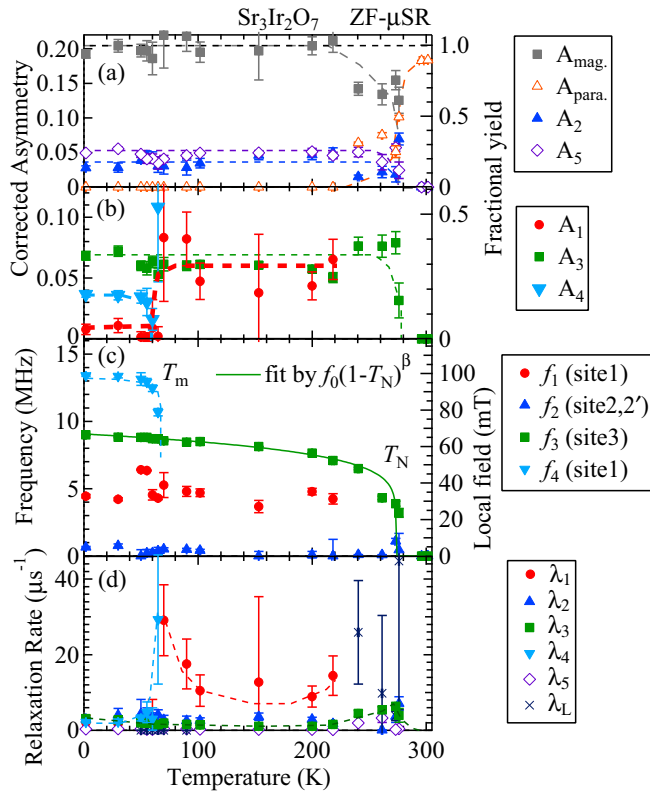FIG. 4. (Color online) Temperature dependence of (a), (b) partial asymmetry, (c) muon precession frequency, and (d) relaxation rate in $Sr_3Ir_2O_7$. Solid curve is fitting line, and dashed curves are visual guides. For the correspondence between f_i and muon sites, see Fig. 7.

small amplitude ($A_3 \simeq 7\%$–12% in Sr_2IrO_4), although it may also be due to the change in the population of muon sites induced by the modulation of the crystal structure upon the substitution of Sr by Ba.

B. $Sr_3Ir_2O_7$

The ZF-μSR spectra in $Sr_3Ir_2O_7$ were described by four components ($i = 1$–3,5) for $T_m < T < T_N$, while another component ($i = 4$) appeared below T_m. Such a two-step behavior is qualitatively parallel to that in Sr_2IrO_4. Figure 4 shows the temperature dependence of A_i, f_i, and λ_i, where f_3 seems to be the primary component reflecting the magnetic order parameter for $T_m < T < T_N$, while the behavior of the other components ($f_1 \simeq 4$ MHz, $f_2 \simeq 0.6$ MHz, and $f_5 \simeq 0$ MHz) is relatively ambiguous. The transition temperature $T_N = 273.7(4)$ K determined by the onset of f_3 showed close agreement with the bulk properties, including the specific heat [10,23]. Curve fitting of f_3 using $f_3(T) = f_{(0)3}(1 - T/T_N)^\beta$ yielded $\beta \simeq 0.143(3)$, which is closer to the value for the 2D-Ising model ($\beta \sim 0.125$) than the case of Sr_2IrO_4. This suggests a stronger 2D characteristic of the magnetic order in $Sr_3Ir_2O_7$.

Although the value of $f_{(0)3}$ [= 9.07(3) MHz] happened to be close to $f_{(0)3}$ in Sr_2IrO_4 [= 8.22(4) MHz], the T_N values determined by these signals clearly differed between the respective compounds. (This in turn indicates that the f_3

component in the Sr_2IrO_4 sample cannot be attributed to the $Sr_3Ir_2O_7$ impurity phase.)

From the appearance of f_4 below $T_m \simeq 70$ K, $Sr_3Ir_2O_7$ was inferred to undergo a secondary magnetic transition for $T < T_m$. The transition was accompanied by a reduction in A_1, which suggests that the signal comes from muons formerly associated with f_1 for $T > T_m$. Furthermore, both λ_1 and λ_4 exhibited a steep increase around T_m, which is regarded as the critical divergence of the relaxation rate often observed for the conventional magnetic order. Figures 2(d) and 2(e) show that the relative amplitude of f_4 ($\propto A_4$) was mostly independent of the temperature in $Sr_3Ir_2O_7$ below T_m. This is in contrast to the case in Sr_2IrO_4, where it increased as the temperature decreased below ~ 30 K. These results suggest that these two phases (or "states") coexist in $Sr_3Ir_2O_7$ below T_m. Thus, while the magnetism of $Sr_3Ir_2O_7$ shares the feature of a secondary phase below T_m with Sr_2IrO_4, the temperature dependence of its order parameter demonstrates one of the differences between these two compounds.

The above results are substantially different from that reported earlier in the literature [21]. Franke *et al.* reported emergence of a single frequency component over a temperature range of $25 \leqslant T \leqslant 160$ K, where the magnitude of the frequency (1.8–2.8 MHz) and its temperature dependence were rather close to that of f_1 in Sr_2IrO_4. In contrast, we found no corresponding signal in the present result for $Sr_3Ir_2O_7$. They also referred to a signal component that exhibits extremely rapid relaxation (~ 40 MHz) over the entire temperature range that they studied ($\leqslant 260$ K), which is missing from our result. These observations suggest that the specimen used by Franke *et al.* [21] may have contained a significant fraction of ingrowth Sr_2IrO_4 phase upon preparation.

C. $SrIrO_3$

Unlike the preceding two cases, $SrIrO_3$ remained nonmagnetic over the entire temperature range studied (2 K $< T <$ 250 K), which was inferred from the absence of a spontaneous muon precession signal in ZF-μSR spectra. More specifically, the spectra shown in Fig. 2(c) are the sum of two components showing Gaussian depolarization due to nuclear random local fields. While the depolarization was mostly quenched by applying a longitudinal magnetic field of 10^1 mT, a slowly depolarizing component remained [see the inset of Fig. 2(c) showing the data at 2 K]. This suggests the presence of residual fast spin dynamics of Ir 5d electrons behind the random local fields from nuclear dipolar moments. The spectra were analyzed by curve fitting using the form

$$A(t) = \sum_{i=1}^{2} A_i G_z(t, \Delta_i) e^{-\lambda_i t}, \qquad (3)$$

which becomes

$$\simeq \sum_{i=1}^{2} A_i \left[\frac{1}{3} + \frac{2}{3} \left(1 - \Delta_i^2 t^2 \right) e^{-\Delta_i^2 t^2 / 2} \right] e^{-\lambda_i t}$$

under a zero field, where Δ_i is the Gaussian relaxation rate determined by the second moment of nuclear dipolar fields and λ_i is the relaxation rate due to the fluctuation of paramagnetic moments. We obtained $\Delta_1 = 0.026(2) \, \mu s^{-1}$ and
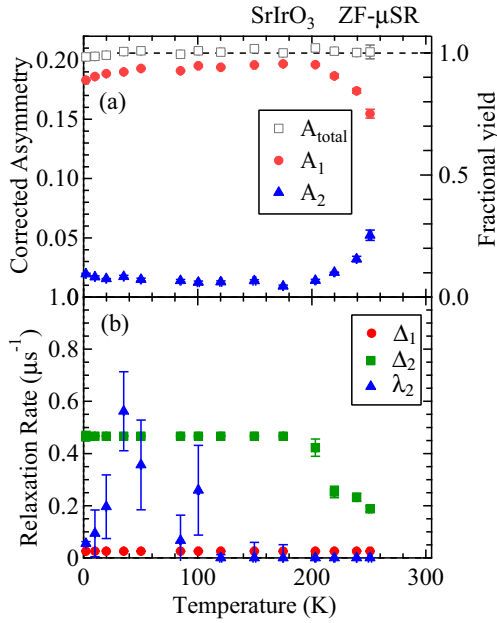
FIG. 5. (Color online) Temperature dependence of (a) partial asymmetry A_i and (b) relaxation rate Δ_i, λ_2 in SrIrO$_3$.

$\Delta_2 \simeq 0.46(2)$ μs^{-1} from the fitted curves, including those under LF-μSR measured at 2 K.

Figure 2(c) shows that the primary component of the time spectra ($A_1 \geqslant 0.18$) did not appreciably change with time nor under different LF. This makes it difficult to reliably determine Δ_1 and λ_1 as independent parameters. A similar difficulty arose for the secondary component from the small signal amplitude ($A_2 \leqslant 0.02$). Consequently, λ_2 alone was treated as a parameter in the curve fitting to determine the temperature dependence of the spectra, while $\Delta_{1,2}$ was fixed to the values determined at 2 K (except for $T > 200$ K where Δ_2 was set free) and λ_1 was fixed to zero. In such a situation, λ_2 extracted from curve fitting would be equivalent to $\lambda_1 \simeq (A_2/A_1)\lambda_2$ under the reverse conditions.

Figure 5 summarizes the analysis results. λ_2 exhibited a weak enhancement around 30–50 K, which may suggest a slowing down of paramagnetic spin fluctuation. This is consistent with the bulk magnetic properties, which are mostly due to paramagnetism. The electronic structure of SrIrO$_3$ is reportedly on the verge of the metal-insulator transition, so the conducting carriers would have a large effective mass because of the strong electronic correlation [3]. At this stage, there were a number of bulk property measurements with anomalies around 30–50 K: the resistivity, Seebeck, and Hall coefficients exhibited a kink at $\sim$45 K, and the Nernst effect showed a peak at $\sim$35 K. These anomalies seem to coincide with the enhancement of λ_2 observed over a similar temperature range.

IV. DISCUSSION

In the magnetically ordered states of Sr$_2$IrO$_4$ and Sr$_3$Ir$_2$O$_7$, the Ir^{4+} isospin state is virtually equivalent to the superposition of a magnetic dipole and octupole for f-electron systems, where the octupole makes a relatively small contribution to reducing the total magnetic induction. Thus, the local field at

the muon site can reasonably be assumed to be predominantly determined by the pointlike magnetic dipoles situated at Ir sites. The internal field B_{loc} at the muon site is given by the vector sum of the dipolar fields exerted from local Ir^{4+} isospin moments:

$$B_{\text{loc}} = \left| \sum_j \hat{\mathbf{A}}_j \boldsymbol{\mu}_j \right|, \qquad (4)$$

where $\hat{\mathbf{A}}_j$ is the dipole tensor and is expressed by

$$\hat{\mathbf{A}}_j = A_j^{\alpha\beta} = \frac{1}{r_j^3} \left(\frac{3\alpha_j \beta_j}{r_j^2} - \delta_{\alpha\beta} \right) \quad (\alpha, \beta = x, y, z). \qquad (5)$$

The summation runs through the jth Ir^{4+} moment $\boldsymbol{\mu}_j$ located at $\boldsymbol{r}_j = (x_j, y_j, z_j)$ from a given muon site. For a given magnetic structure and Ir^{4+} moment size, B_{loc} can be calculated for comparison with the observed

$$B_i = 2\pi f_i / \gamma_\mu.$$

The local electronic state associated with a muon is virtually identical with that of hydrogen as an interstitial atom because the difference in the reduced mass of the electron bound to the muon (which determines the Bohr atomic radius) is only $\sim$0.5% compared with that of hydrogen. Moreover, in transition metal (TM) oxides, the energy level of the electronic state associated with interstitial hydrogen $E^{+/-}$ has been empirically established to be predominantly determined by a common offset of nearly -3 eV measured from the vacuum level regardless of the host compounds [24,25]; the muon is predicted to stay diamagnetic (accompanying no unpaired spin density) as long as $E^{+/-} > E_c$ (where E_c is the energy at the bottom of the conduction band). This is perfectly in line with the common observation that the muon in TM oxides satisfying the condition $E^{+/-} > E_c$ tends to form an O-μ covalent bond (a muonic analog of the OH bond), where the local O-μ binding energy is the primary factor that determines $E^{+/-}$. Because Sr$_{n+1}$Ir$_n$O$_{3n+1}$ has a relatively narrow band gap (i.e., E_c is far below the vacuum level, so $E^{+/-} > E_c$), we can safely presume that the muon forms an O-μ bond in these Ir compounds. Accordingly, we searched for muon sites bound to oxygen (with a typical O-μ distance of $\sim$0.1 nm) in the respective compounds that are situated near the (local) minima of the electrostatic potential that are induced by local ions.

The electrostatic potential was calculated using a custom-made computer program assuming a point charge for each atom [26], where the valence state and lattice structure were the input parameters. In addition, the Vienna *Ab initio* Simulation Package [27] (VASP; codes for the *ab initio* quantum mechanical molecular dynamics calculation) was used to examine the validity of the potential minima derived from the calculation based on the point-charge approximation. These calculations showed perfect agreement for the case of Sr$_2$IrO$_4$, while a slight difference was suggested for Sr$_3$Ir$_2$O$_7$ and SrIrO$_3$ (see below).

In the paramagnetic state, the muon-Ir^{4+} hyperfine parameter (which is predominantly determined by the magnetic dipolar interaction) is estimated by calculating the second
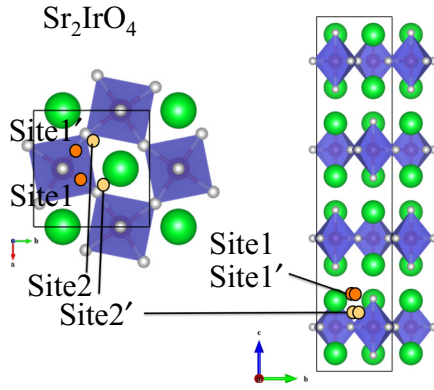
FIG. 6. (Color online) Presumed muon sites in Sr_2IrO_4. Site 1 and site 1' are close to apical oxygen (O1), and site 2 and site 2' are near the IrO_2 plane (O2).

moment

$$A_\mu^2 = \sum_{j,\alpha,\beta} \left[\left(A_j^{\alpha\beta} \right) \mu_j^\beta \right]^2 \; (\alpha = x,y, \; \beta = x,y,z), \qquad (6)$$

where the sum runs over the α and β components of the terms exerting a magnetic field perpendicular to initial muon polarization from the jth nuclear magnetic moment. The nuclear dipolar width (Δ^2/γ_μ^2) can be estimated with the above equation by substituting μ_j with those of the nuclear magnetic moments.

In the following, the assignment of muon sites is discussed through a comparison of B_i and the calculated values of B_{loc} in Sr_2IrO_4 and $Sr_3Ir_2O_7$. In contrast, it is solely based on Δ in $SrIrO_3$ because the compound remained paramagnetic for the entire temperature range considered in the present study.

A. Sr_2IrO_4

We adopted a canted AF structure (with μ_j tilted by 11° from the a axis) and the Ir moment size determined from RXD and neutron diffraction measurements ($|\mu_j| \simeq 0.36\mu_B$) in Sr_2IrO_4. We further assumed that the relevant magnetic structure is realized over the temperature region $T_m < T < T_N$. Then, considering that there are two crystallographically inequivalent oxygen sites, i.e., apical oxygen (O1) and in-plane oxygen (O2), the comparison between f_i and $f_\mu \equiv \gamma_\mu B_{loc}$ yields a consistent set of muon sites. This is shown in Fig. 6, where f_1 and f_2 correspond to muons bound to O1 (site 1 and site 1'), whereas f_3 is associated with those bound to O2 (site 2) (see Table I for more details). The magnitude of A_i represents the initial distribution of implanted muons among the corresponding sites. The Ir^{4+} moment size is commonly estimated to be $\sim 0.4\mu_B$ from the magnitude of frequencies for all muon sites, which closely agrees with the value inferred from RXD data for $T_m < T < T_N$.

For the in-plane oxygen (O2), our calculation of the electrostatic potential predicted another set of sites with lower potential energy than site 2. The corresponding hyperfine parameters calculated from the dipole tensor were 256.4/248.1 mT/μ_B. Thus, a μSR frequency of 13.9/13.5 MHz is predicted for the Ir moment size of $\sim 0.4\mu_B$. We presumed that the corresponding μSR signal may not have been resolved in the present μSR

time spectra because of the small amplitude and/or fast depolarization based on the achieved statistical precision. The small reduction of the total asymmetry (A_{mag}) observed below T_m (see Fig. 3) also suggests that an unresolved (missing) signal exists.

These site assignments with the presumed Ir moment size do not necessarily correlate with the distinct features observed below T_m (see Fig. 3): (i) f_1 splits into two lines, and (ii) they exhibit a divergent increase below ~ 40 K. It is unlikely that feature (i) can be explained by further canting of the Ir isospin moments (i.e., from $\sim 11°$ to $\sim 13°$ within the ab plane inferred from x-ray and neutron diffraction [2,8]) because the expected change in $f_{1,2}$ induced by such a canting (~ 0.088 MHz) would be too small to explain the observed change. We also investigated a variety of possibilities for magnetic structures, including the spin flop from the ab-in-plane to the c-parallel configuration (as has been suggested to occur upon Mn substitution for Ir by 10%) [28]. However, we found that the calculated f_μ was far below the observed change of $f_{1,2}$ up to 4–5 MHz for any arbitrary spin configuration.

The change of $f_{1,2}$ below ~ 40 K also cannot be attributed to the increase of the Ir isospin moment size (without a change in the magnetic structure), because this would lead to an enhancement of f_3, which is also proportional to the Ir moment size ($\propto$ order parameter). Figure 3 clearly shows that f_3 does not exhibit divergent behavior that is in marked contrast to $f_{1,2}$.

These observations have led us to postulate that the magnetism below T_m is associated with the development of spin polarization at the relevant oxygen sites. We discuss this possibility in the next section in detail.

B. $Sr_3Ir_2O_7$

There are three crystallographically inequivalent oxygen sites in $Sr_3Ir_2O_7$: the outer apical oxygen (O1), IrO_2 in-plane oxygen (O2), and inner apical oxygen shared by two IrO_6 octahedra (O3). Assuming the occurrence of an O-μ bond common to the case in Sr_2IrO_4, we investigated potential minima for the μ^+ around each oxygen that also meets the criterion that the Ir moment sizes estimated from the magnitude of B_{loc} for different sites agree with each other (given that the Ir moment size is uniform). Figure 7 shows the results,
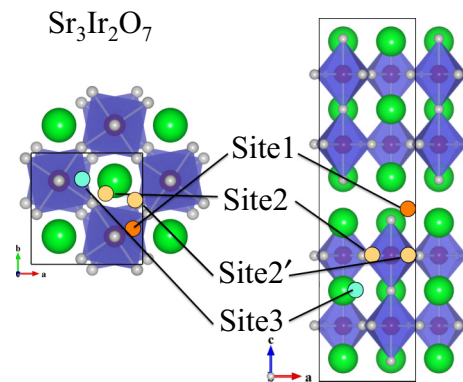

FIG. 7. (Color online) Presumed muon sites in $Sr_3Ir_2O_7$. Site 1 is close to apical oxygen (O1), sites 2 and 2' are near IrO_2 planes (O2, O2'), and site 3 is near the shared apical oxygen (O3).

TABLE II. Muon spin precession frequency (f_i) in the AF phase of $Sr_3Ir_2O_7$. While f_3 can be extrapolated to $T = 0$ by curve fitting using the form $f_{(0)3}(1 - T/T_N)^\beta$ for $T_m \leqslant T \leqslant T_N$), other components only allow a simple linear extrapolation with considerable uncertainty because of the relatively large scattering of data (see Fig. 4). Regarding the double value of f_2, refer to the main text. The Ir moment size is estimated with the equation $\mu_{Ir} = B_{loc}/\overline{B}_{loc}$, where $\overline{B}_{loc}$ is the field calculated for the Ir moment size of $1\mu_B$. Muon sites were assigned by searching for the position of local potential minima around oxygen (with a distance of 0.1 nm), where the corresponding μ_{Ir} are reasonably close to each other. (The position is given in polar coordinates with the $\hat{z}$ axis parallel to the crystalline c axis.) O1: outer apical oxygen (0.75, 0.25, 0.1943); O2: in-plane oxygen (0.5487, 0.5485, 0.0962); O2′: in-plane oxygen (0.0487, 0.4515, 0.3462); O3: shared apical oxygen (0.5, 0.25, 0).

Site	i	$f_{(0)i}$ (MHz)	B_i (mT)	T_N (K)	β	μ^+ position (θ, ϕ)	$\overline{B}_{loc}$ (mT/μ_B)	μ_{Ir}
1	1	4.5(5)	33.2(37)			O1 + (60°, 45°)	92.0	0.36(4)μ_B
2	2	0.30(8)	2.2(6)			O2 + (90°, 45°)	8.06	0.28(7)μ_B
2′	2	0.70(5)	5.2(4)			O2′ + (90°, 135°)	17.9	0.29(2)μ_B
3	3	9.07(3)	66.9(2)	273.7(4)	0.143(3)	O3 + (90°, 45°)	215.5	0.310(1)μ_B

where f_1 corresponds to O1 (site 1, near the outer apical O), f_2 corresponds to O2 (site 2, close to in-plane O), and f_3 corresponds to muons bound to O3 (site 3, near the shared apical O; refer to Table II for more details). We also note that f_2 tended to converge to two different frequencies, although it was difficult to extract these two values simultaneously from curve fitting. We interpreted this as a trace of a signal from another site near O2 (site 2′) that was barely resolved. Interestingly, the VASP calculation suggests that site 2′ is 0.13 nm away from O2 (whereas the point charge approximation suggests 0.1 nm), which would reduce B_{loc} to 14.3 mT. However, such a small difference would be hard to identify in the present data.

In addition, we tested three possible AF structures, i.e., those collinear with one of three crystal axes (a, b, or c), and found that the one collinear with the c axis met the criterion. The structure showed perfect agreement with that inferred from RXD measurements [12,13], which supports our assumption that the muon sites were correctly identified. Consequently, the Ir moment size was determined to be $\sim 0.31(2)\mu_B$ from the average μ_{Ir} for sites 1–3.

At this stage, the origin of the secondary transition at $T_m = 70$ K inferred from the appearance of f_4 is unclear. While the amplitude of f_4 (A_4) developed in place of that for f_1 (A_1, the signal from muons bound to the apical oxygen), it showed no correlation with other frequency signals that remained unchanged as the temperature passed through T_m. As is the case for Sr_2IrO_4 below T_m, neither the change in the Ir moment orientation nor in its moment size can explain such a behavior. Attempts to attribute the observed change to a variety of modulated Ir moment orientation/size always lead to a change in B_{loc} for all muon sites, which is inconsistent with the current experimental observation.

The development of anomalous internal field is commonly observed with muons at the near-apical oxygen site in both Sr_2IrO_4 and $Sr_3Ir_2O_7$. As suggested previously, we now speculate that this is in accordance with the development of ordered magnetic moments at the relevant oxygen site, which is common to these two compounds (see below).

C. SrIrO₃

The number of crystallographically inequivalent oxygen is reduced to two in the orthorhombic $SrIrO_3$, which is similar to Sr_2IrO_4 except that the apical oxygen (O1) is shared by two IrO_6 octahedra. In this situation, there are two possible

muon sites for the presumed O-μ bonding (see Fig. 8), just like for Sr_2IrO_4. The muon sites were searched for by calculating the electrostatic potential using lattice parameter and atomic coordinates for the orthorhombic perovskite $SrIrO_3$ with $Pbnm$ crystal symmetry [16,18]. We obtained a potential minimum for each oxygen atom (site 1 for O1 and site 2 for O2; see Table III).

As noted earlier, the analysis of LF-μSR data yielded $\Delta_1 = 0.026(2)$ μs^{-1} and $\Delta_2 = 0.46(2)$ μs^{-1} for each signal component. However, the calculated line width turned out to be nearly the same for these sites with $\Delta \simeq 0.024-0.026$ μs^{-1}. We also found that calculation using VASP codes predicted another potential minimum situated at the center of four apical oxygen atoms, for which $\Delta \simeq 0.022$ μs^{-1}. While these values of Δ closely agree with Δ_1 (corresponding to the predominant signal), there is a large discrepancy with Δ_2. Note that Δ never exceeded 0.20 μs^{-1} at any available interstitial site (regardless of the likelihood of occupancy according to the electrostatic potential). This suggests that the signal corresponding to Δ_2 does not come from $SrIrO_3$ but from an unidentified impurity phase. However, we stress that the volumetric fraction of this phase was less than $\sim 10\%$ below ~ 200 K (see Fig. 5), which indicates that the Pauli paramagnetic behavior can be attributed to the predominant fraction making up the $SrIrO_3$ phase.

The muon-Ir hyperfine parameter (A_μ) in $SrIrO_3$ as a paramagnetic metal can be estimated by calculating the dipolar sum using Eq. (6). Table III summarizes the results. A_μ was found to take similar values for those two muon sites ($\simeq 10^2$ mT/μ_B). Considering that the muon depolarization rate under spin fluctuation can be approximated with the
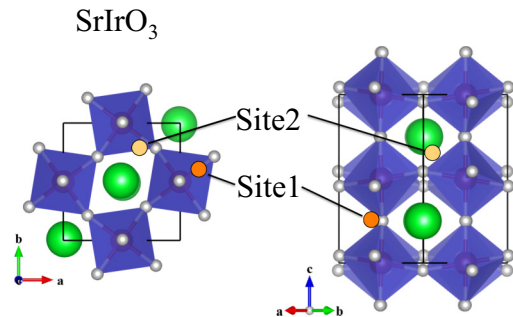

FIG. 8. (Color online) Presumed muon sites in $SrIrO_3$. Site 1 is close to apical oxygen (O1), and site 2 is near IrO_2 planes (O2).

TABLE III. Muon site assignment in SrIrO$_3$ made by locating the potential minimum around oxygen (with a distance of 0.1 nm), where the nuclear dipolar line width (Δ) is consistent with experimental observation. (The muon position is given in polar coordinates with the $\hat{z}$ axis parallel to the crystalline c axis.) O1: share apical oxygen (0.9940, 0.5073, 0.2500); O2: in-plane oxygen (0.7920, 0.7860, 0.5440).

Site	μ^+ position (θ,ϕ)	Δ_i (μs^{-1})	A_μ (mT/μ_B)
1	O1 + (90°,31°)	0.0241	105.4
2	O2 + (13°,180°)	0.0250	90.2

Redfield theory of spin relaxation

$$\lambda \simeq \frac{\gamma_\mu^2 A_\mu^2}{\nu} \qquad (7)$$

and that no appreciable depolarization was observed in this compound within the time window of the observation (i.e., $\lambda < 10^{-2}\ \mu$s^{-1}), we may be able to place a lower bound for the Ir spin fluctuation rate:

$$\nu > 10^{11}\ \text{s}^{-1}. \qquad (8)$$

Assuming that SrIrO$_3$ can be understood as a normal metal (despite it being rather close to a semimetal with a small number of carriers), the spin fluctuation due to the Pauli paramagnetism can be estimated as

$$\nu \simeq \frac{1}{\hbar D(\varepsilon_F)} = \frac{2\pi^2 k_B^2 N_A}{3\hbar\gamma_e} \simeq 2.9 \times 10^{12}\ \text{s}^{-1}, \qquad (9)$$

where $D(\varepsilon_F)$ is the density of state at the Fermi level, N_A is the Avogadro number, and $\gamma_e = 2.45$ mJ/mol K^2 is the Sommerfeld coefficient [17]. This is also consistent with the present experimental result where virtually no appreciable depolarization was observed.

D. Magnetism below T_m

As noted earlier, our extensive survey on the magnetic structure vs B_{loc} in Sr$_2$IrO$_4$ and Sr$_3$Ir$_2$O$_7$ indicated that the internal field observed below T_m cannot be explained by the alteration of the Ir^{4+} isospin configuration from that established above T_m (in contrast to the suggestion in the previous report [21]). The main difficulty lies in the fact that such a scenario always leads to the modulation of B_{loc} at every muon site, whereas only those muons situated near the apical oxygen (O1) actually detected an increase of B_{loc} below T_m.

Given this situation, one of the simplest hypotheses to explain such an observation would be the emergence of ordered magnetic moments on the apical oxygen. In general, the d-electron orbitals are strongly hybridized with p orbitals of the ligand oxygen, which makes it plausible to have an unpaired hole on the oxygen atoms under strong electronic correlation. The small Ir moment in the iridium compounds ($\simeq 0.3-0.4\ \mu_B$) probably originates from the Ir d–O p hybridization in addition to quantum fluctuations. Such a covalency effect has been observed in potassium chloroiridate (K$_2$IrCl$_6$, antifluorite crystal structure), where $\sim$30% of the transferred moment is localized on the apical Cl sites of IrCl$_6$ octahedra [29]. Similar examples have also been found
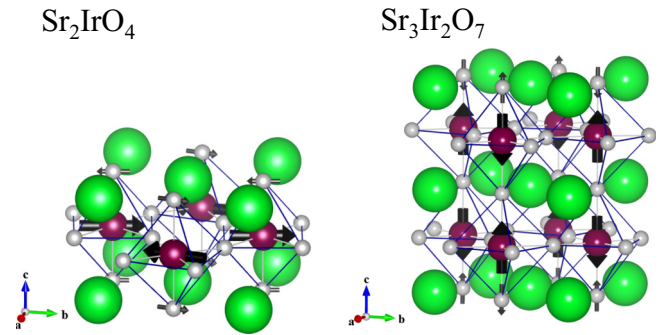
in a variety of compounds including K$_2$CuF$_4$ (Ref. [30]), La$_{0.8}$Sr$_{0.2}$MnO$_3$ (Ref. [31]), La$_5$Ca$_9$Cu$_{24}$O$_{41}$ (Ref. [32]), and Li$_2$CuO$_2$ (Ref. [33]).

Moreover, the rotation of IrO$_6$ octahedra and associated changes in the Ir-O-Ir bond angle at lower temperatures [4,15] may modify the d-p hybridization, and eventually lead to oxygen polarization below T_m.

The possibility of attributing the observed change of B_{loc} to the spin polarization of apical oxygen (O1) was examined in a simulation of B_{loc} assuming a pointlike magnetic dipole $\boldsymbol{\mu}_O$ at each O1 site with its direction antiparallel to the nearest Ir isospin moment (see Fig. 9). B_{loc} was obtained by adding the dipolar fields from O1 to that from Ir (with a moment size of $0.4\mu_B$ in Sr$_2$IrO$_4$ and $0.3\mu_B$ in Sr$_3$Ir$_2$O$_7$). Table IV summarizes the results. The size of $\boldsymbol{\mu}_O$ ($= \mu_O$) was as small as 0.02–0.03 μ_B, which can explain the change in B_{loc} at site 1 and site 1′ in Sr$_2$IrO$_4$ while B_{loc} at the other muon sites was virtually unaffected (relative change of a few percent or less). It also provides a means to map f_1 and f_2 properly to site 1 and site 1′, as B_{loc} was greater at the site 1′ than at the site 1. The results of a simulation under a similar assumption for Sr$_3$Ir$_2$O$_7$ suggest that $\mu_O \simeq 0.09\mu_B$ at the O1 site sufficiently explains the magnitude of f_4. A simulation assuming a ferromagnetic correlation between $\boldsymbol{\mu}_O$ and $\boldsymbol{\mu}_{Ir}$ yielded a similar result, except that B_{loc} at site 2/2′ and site 3 tended to show a slight increase.

The origin of the difference in the temperature dependence between $f_{1,2}$ in Sr$_2$IrO$_4$ and f_4 in Sr$_3$Ir$_2$O$_7$ below T_m is yet

FIG. 9. (Color online) Presumed structure of oxygen magnetic moments associated with apical oxygen (O1) in (a) Sr$_2$IrO$_4$ and (b) Sr$_3$Ir$_2$O$_7$. Oxygen moments are antiparallel with those of iridium in each compound.

TABLE IV. Summary of simulation for B_{loc} in Sr$_2$IrO$_4$ and Sr$_3$Ir$_2$O$_7$ assuming a pointlike magnetic dipolar moment (μ_O) placed on the apical oxygen with their orientation antiparallel to Ir moment (with Ir moment size of $0.4\mu_B$ in Sr$_2$IrO$_4$ and $0.3\mu_B$ in Sr$_3$Ir$_2$O$_7$). The values of f_i are those linearly extrapolated to $T = 0$.

	Site	i	f_i (MHz)	B_i (mT)	μ_O	B_{loc} (mT)
	1	1	$\sim$4.5	$\sim$33		35.7
Sr$_2$IrO$_4$	1′	2	$\sim$3.9	$\sim$29	$0.025\mu_B$	26.4
	2	3	8.22(4)	60.6(3)		60.1
	1	4	13.4(1)	98.9(1)		102.0
Sr$_3$Ir$_2$O$_7$	2/2′	2	0.3–0.7	2.2–5.2	$0.09\mu_B$	1.6–2.8
	3	3	9.07(3)	66.9(2)		63.1

to be identified. It is clearly related with the origin of f_4 in Sr_2IrO_4 that emerges prior to $f_{1,2}$ with decreasing temperature. The long-range structure of oxygen moments just below T_m in Sr_2IrO_4 may differ from that at the lowest temperature. The magnitude of μ_O is another factor that may determine the effective interaction between oxygen moments. A small μ_O in Sr_2IrO_4 would make it more difficult to establish a long-range order than that in $Sr_3Ir_2O_7$.

Such a difference between Sr_2IrO_4 and $Sr_3Ir_2O_7$ is a strong argument against the alternative scenario that the observed behavior below T_m is due to the migration of muons from one site to another by thermal activation. This is because there seems to be no obvious reason for the difference in activation energy (which would be mostly determined by the muon binding energy to the apical oxygen) between these two cases.

The possibility of muon-induced local modification to the magnetic structure is also unlikely. Considering the number of implanted muons (one in the specimen at each positron decay measurement using a continuous beam), such a local change (just around the implanted muon) would have difficulty with inducing a well-defined thermodynamical phase having a different transition temperature (T_m) from that of the bulk (T_N).

The present model is also supported by the fact that, assuming an anitferromagnetic interaction between $\boldsymbol{\mu}_O$ and $\boldsymbol{\mu}_{Ir}$ (as might be expected for the nearly $180°$ O-Ir-O bond angle), the reduction in the uniform magnetization below $T_M \sim 100\,K$ in Sr_2IrO_4 and $T_D \sim 50\,K$ and in $Sr_3Ir_2O_7$ (Refs. [14,15]) can be qualitatively understood to be a result of its partial cancellation by oxygen polarization.

One note of interest is a recent example of the manganese compound $TbMn_2O_5$, where an antiferromagnetic spin polarization at the oxygen sites was observed with oxygen K-edge resonant x-ray scattering [34]. The compound exhibited an incommensurate antiferromagnetic order below 43 K that was associated with ferroelectric polarization because of the strong magnetoelectric coupling. It also showed the development of oxygen spin polarization below 38 K, where the dielectric constant exhibited a peak, and the origin of such multiferroic behavior was attributed to a charge redistribution around the ion nucleus in accordance with the alteration of the spin configuration, where spin polarization of the oxygen is a crucial component in the relevant theoretical model [35]. The situation seems to be parallel to the case of Sr_2IrO_4 for which a similar anomaly in the dielectric constant was reported around 70–80 K, which is near T_m [14].

V. CONCLUSION

We used μSR to show that Sr_2IrO_4 and $Sr_3Ir_2O_7$ exhibit clear signs of a two-stage magnetic order, whereas $SrIrO_3$ stays a nonmagnetic metal. Provided that the predominant muon sites are located near the oxygen atoms common to these two compounds and that the effective Ir moment size is 0.3–0.4 μ_B, the magnitude of B_{loc} in the first-stage order ($T_m \leqslant T \leqslant T_N$) closely agrees with that predicted from the magnetic structures of each compound, which were recently inferred from resonant x-ray and neutron diffraction. For the secondary magnetic phase emerging below T_m, we postulate that it originates from ordered magnetic moments ($\sim 0.03\mu_B$ in Sr_2IrO_4 and $\sim 0.09\mu_B$ in $Sr_3Ir_2O_7$) at the apical oxygen of the IrO_6 octahedron, which is induced by strong hybridization of Ir d–O p orbitals. This hypothesis provides a qualitative explanation for the reported anomalies in both the magnetic and dielectric properties over the relevant temperature range according to the earlier literature. A neutron diffraction study is currently underway to confirm the oxygen magnetic moments in those compounds.

The present results demonstrate the usefulness of the μSR technique in investigating local magnetism associated with oxygen, and it has the potential to be widely applicable to strongly correlated transition metal oxides owing to the fact that implanted muons tend to form a well-defined O-μ bonding state as interstitial pseudohydrogen atoms in oxides.

[1] B. J. Kim, Hosub Jin, S. J. Moon, J.-Y. Kim, B.-G. Park, C. S. Leem, Jaejun Yu, T. W. Noh, C. Kim, S.-J. Oh, J.-H. Park, V. Durairaj, G. Cao, and E. Rotenberg, Phys. Rev. Lett. **101**, 076402 (2008).

[2] B. J. Kim, H. Ohsumi, T. Komesu, S. Sakai, T. Morita, H. Takagi, and T. Arima, Science **323**, 1329 (2009).

[3] S. J. Moon, H. Jin, K. W. Kim, W. S. Choi, Y. S. Lee, J. Yu, G. Cao, A. Sumi, H. Funakubo, C. Bernhard, and T. W. Noh, Phys. Rev. Lett. **101**, 226402 (2008).

[4] M. K. Crawford, M. A. Subramanian, R. L. Harlow, J. A. Fernandez-Baca, Z. R. Wang, and D. C. Johnston, Phys. Rev. B **49**, 9198 (1994).

[5] T. Shimura, Y. Inaguma, T. Nakamura, M. Itoh, and Y. Morii, Phys. Rev. B **52**, 9143 (1995).

[6] G. Cao, J. Bolivar, S. McCall, J. E. Crow, and R. P. Guertin, Phys. Rev. B **57**, R11039 (1998).

[7] S. W. Lovesy, D. D. Khalyavin, P. Manuel, L. C. Chapon, G. Cao, and T. F. Qi, J. Phys.: Condens. Matter **24**, 496003 (2012).

[8] F. Ye, S. Chi, B. C. Chakoumakos, J. A. Fernandez-Baca, T. Qi, and G. Cao, Phys. Rev. B **87**, 140406(R) (2013).

[9] G. Jackeli and G. Khaliullin, Phys. Rev. Lett. **102**, 017205 (2009).

[10] G. Cao, Y. Xin, C. S. Alexander, J. E. Crow, P. Schlottmann, M. K. Crawford, R. L. Harlow, and W. Marshall, Phys. Rev. B **66**, 214412 (2002).

[11] S. Boseggia, R. Springell, H. C. Walker, A. T. Boothroyd, D. Prabhakaran, S. P. Collins, and D. F. McMorrow, J. Phys.: Condens. Matter **24**, 312202 (2012).

[12] J. W. Kim, Y. Choi, Jungho Kim, J. F. Mitchell, G. Jackeli, M. Daghofer, J. van den Brink, G. Khaliullin, and B. J. Kim, Phys. Rev. Lett. **109**, 037204 (2012).

[13] S. Fujiyama, K. Ohashi, H. Ohsumi, K. Sugimoto, T. Takayama, T. Komesu, M. Takata, T. Arima, and H. Takagi, Phys. Rev. B **86**, 174414 (2012).

[14] S. Chikara, O. Korneta, W. P. Crummett, L. E. DeLong, P. Schlottmann, and G. Cao, Phys. Rev. B **80**, 140407(R) (2009).

[15] L. Li, P. P. Kong, T. F. Qi, C. Q. Jin, S. J. Yuan, L. E. DeLong, P. Schlottmann, and G. Cao, Phys. Rev. B **87**, 235127 (2013).

[16] J. G. Zhao, L. X. Yang, Y. Yu, F. Y. Li, R. C. Yu, Z. Fang, L. C. Chen, and C. Q. Jin, J. Appl. Phys. **103**, 103706 (2008).

[17] K. Ohashi, T. Takayama, and H. Takagi (unpublished).

[18] J. M. Longo, J. A. Kafalas, and R. J. Arnott, J. Solid State Chem. **3**, 174 (1971).

[19] S. Fujiyama (private communication).

[20] R. S. Hayano, Y. J. Uemura, J. Imazato, N. Nishida, T. Yamazaki, and R. Kubo, Phys. Rev. B **20**, 850 (1979).

[21] I. Franke, P. J. Baker, S. J. Blundell, T. Lancaster, W. Hayes, F. L. Pratt, and G. Cao, Phys. Rev. B **83**, 094416 (2011).

[22] H. Okabe, M. Isobe, E. Takayama-Muromachi, A. Koda, S. Takeshita, M. Hiraishi, M. Miyazaki, R. Kadono, Y. Miyake, and J. Akimitsu, Phys. Rev. B **83**, 155118 (2011).

[23] I. Nagai, Y. Yoshida, S. I. Ikeda, H. Matsuhata, H. Kito, and M. Kosaka, J. Phys.: Condens. Matter **19**, 136214 (2007).

[24] Ç. Kiliç and A. Zunger, Appl. Phys. Lett. **81**, 73 (2002).

[25] S. F. Cox, J. L. Gavartin, J. S. Lord, S. P. Cottrell, J. M. Gil, H. V. Alberto, J. Piroto Duarte, R. C. Viläo, N. Ayres de Campos, D. J. Keeble, E. A. Davis, M. Charlton, and D. P. van der Werf, J. Phys.: Condens. Matter **18**, 1079 (2006).

[26] K. M. Kojima, J. Yamanobe, H. Eisaki, S. Uchida, Y. Fudamoto, I. M. Gat, M. I. Larkin, A. Savici, Y. J. Uemura, P. P. Kyriakou, M. T. Rovers, and G. M. Luke, Phys. Rev. B **70**, 094402 (2004).

[27] See, for example, http://www.vasp.at.

[28] S. Calder, G.-X. Cao, M. D. Lumsden, J. W. Kim, Z. Gai, B. C. Sales, D. Mandrus, and A. D. Christianson, Phys. Rev. B **86**, 220403(R) (2012).

[29] J. W. Lynn, G. Shirane, and M. Blume, Phys. Rev. Lett. **37**, 154 (1976).

[30] K. Hirakawa and H. Ikeda, Phys. Rev. Lett. **33**, 374 (1974).

[31] J. Pierre, B. Gillon, L. Pinsard, and A. Revcolevschi, Europhys. Lett. **42**, 85 (1998).

[32] M. Matsuda, K. M. Kojima, Y. L. Uemura, J. L. Zaretsky, K. Nakajima, K. Kakurai, T. Yokoo, S. M. Shapiro, and G. Shirane, Phys. Rev. B **57**, 11467 (1998).

[33] E. M. L. Chung, G. J. McIntyre, D. McK. Paul, G. Balakrishnan, and M. R. Lees, Phys. Rev. B **68**, 144410 (2003).

[34] T. A. W. Beale, S. B. Wilkins, R. D. Johnson, S. R. Bland, Y. Joly, T. R. Forrest, D. F. McMorrow, F. Yakhou, D. Prabhakaran, A. T. Boothroyd, and P. D. Hatton, Phys. Rev. Lett. **105**, 087203 (2010).

[35] A. S. Moskvin and R. V. Pisarev, Phys. Rev. B **77**, 060102(R) (2008).